Journal of Manufacturing Engineering, September, 2012, Vol. 7, Issue. 3, pp 129-133

TEXTURAL ANALYSIS OF FexZn(1–x) ALLOYS FORMED BY ELECTRODEPOSITION AND SOL-GEL TECHNIQUES

*** Kanagasabapathy M[1], Sivan R[2], Perumal S[3] and Sivaramamoorthy K[4]**

[1]Department of Chemistry, Rajapalayam Rajus' College, Rajapalayam, Tamil Nadu-626 117, India
[2,3]Physics Research Centre, S.T.Hindu College, Nagercoil, Tamil Nadu- 629 002, India
[4]Department of Physics, Rajapalayam Rajus' College, Rajapalayam, Tamil Nadu-626 117, India

ABSTRACT

Crystallographic textural analysis of $Fe_xZn_{(1–x)}$ alloys formed by electrodeposition and sol–gel techniques was done. Lattice parameters and phase structures of the alloys were elucidated and correlated to empirical composition. In electrodeposited alloy 101 pyramidal plane is dominant with 'η' (distorted hcp) phase structure, whereas the alloy formed under sol–gel conditions has significant 002 basal plane orientation with 'Γ' phase structure. HCP Lattice distortion is not observed for alloys from sol–gel method. Crystallite size and internal average strain was lower for the alloys obtained from sol–gel method. However, due to epitaxial nucleation by Zn ad-atoms and the selective precipitation of 'η' phase over 'δ' phase, the lattice orientation is more uniform and dense packed for electrodeposited alloys.

Keywords: Fe–Zn alloy, Electrodeposition and Sol-gel.

1. Introduction

Iron-zinc alloys are gaining greater industrial significance in recent years, due to their potential engineering applications in the fields of steel corrosion prevention, automobile, aircraft, military, magnetic and lithium battery components processing etc., since they are having relatively better tensile strength, hardness, weldability, abrasion resistance, formability, corrosion resistance and other surface engineering characteristics than their metal counterparts [1–3]. These engineering characteristics are due to the unique phase structure of the alloy formed by the substitution of iron in zinc hcp lattice, and are entirely differ from thermal equilibrium phase structure [4].

The technological application of an alloy depends on its phase structure and textural orientations. For instance, Fe_5Zn_{24} with dominant 0002 crystallographic orientations and 'η'hcp phase structure has three times higher corrosion resistance than galvanized coatings, but $Fe_2Zn_{1.68}$ with 101 orientations and 'δ' phase has twice the microhardness, phosphatability, weldability and tensile strength than the galvanized coatings [5, 6]. But no reports are available to correlate the crystallographic textural characteristics with empirical phase composition of alloy formed by electrodeposition as well as sol-gel techniques. This work addresses lattice parameter analysis of $Fe_xZn_{(1–x)}$ alloy formed by electrochemical and sol-gel methods.

2. Experimental Procedure

Electrodeposition of iron–zinc alloy was carried out [6] from the sulphate bath. The bath composition is as follows: $[ZnSO_4.7H_2O]$ – 0.3 M; $[FeSO_4\ (NH_4)_2SO_4\ 6H_2O]$ – 0.5 M and [KCl] – 1.0 M. In the bath, KCl was added to enhance the bath specific conductance, secondary and tertiary current distribution. Deposition was done over mechanically polished and electro-cleaned mild steel panels of size 5.0 cm × 2.5 cm × 0.05 cm, under galvanostatic conditions by three electrode assembly, using DC rectifier, (Aplab L3230 model, India make). Current density was varied from 1 to 5 A/dm^2 with 0.5 $A.dm^2$ variations. The anode used was electrolytic grade (99.99%) zinc, with same dimensions of cathode.

Sol-gel method followed to form $Fe_xZn_{(1–x)}$ is similar to combustion technique adopted by Kanagesan et al.,[7] with D-fructose as a fuel. Analytical grade Zn $(NO_3)_2$ (CDH, 99%) and Fe $(NO_3)_3{\cdot}9H_2O$ (CDH, 99.65%) and D–Fructose (SD fine, 99.9%) were used as starting materials. Both metal nitrates and fuel were dissolved in distilled water and stirred in mechanical stirrer for 2 h . Then sol was heated at 80°C with stirring and finally it became sticky liquid gel. It was preheated at 130°C in a hot air oven for two days to get precursor powder. The precursor was calcinated at 900°C for 3 h.

**Corresponding Author - E- mail: rrcmks@gmail.com*

Composition of the alloy was analysed by Energy Dispersive X–ray Analyser (Hitachi S–3000H model). X-ray diffraction analysis was carried out by, PANalytical X'per PRO model using CuK_α radiation at 45kV and 40 mA (λ = 1.5406 A^o) in a wide range of 2θ ($10° < 2\theta < 80°$) at a rate of 1^o min^{-1}. Scanning electron microscopic (SEM) images were obtained by using Hitachi S–3000H model.

3. Results and Discussion

3.1 Computational analysis of hkil, 'c' and 'a'

The hkl values were interpreted in accordance with ICDD [8]. To interpret the hkil planes along with axial ratio and 'c' and 'a' of distorted hcp lattice parameter from from 2θ, indigenously designed computer program, named 'Crystal FZ' [9] was used [Fig. 1]. By iterations, both hkil for hcp and hkl for bcc can be computed along with d–spacing with <1 % deviation. All the diffracted 2θ angles for the $Fe_xZn_{(1-x)}$, can be indexed from this Crystal FZ. For instance, the basal 004 plane observed at 77^o, for the distorted HCP was indexed through the computation, which is not reported elsewhere.

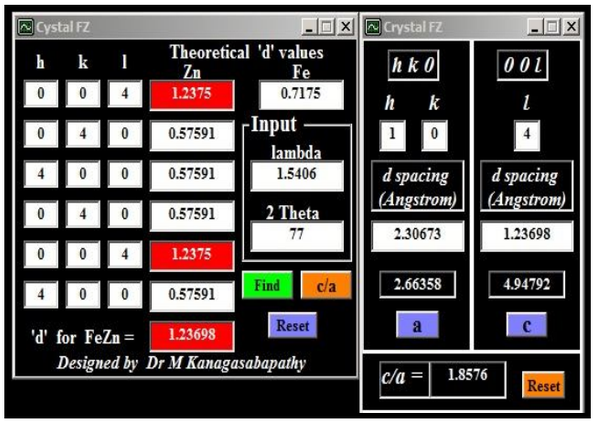

Fig.1 Crystal FZ for hkil, 'c' & 'a' Iterations

3.2 Textural analysis of electrodeposits

Fig. 2 represents the some of XRD patterns of deposits obtained from electrodeposition method by the variation in current density. For electrodeposits the pyramidal textural intensity was significant than the prismatic planes. Unlike sol–gel method the (101) hcp plane at a 2θ of 39.135^o was present in all samples with significant intensity. Current density significantly influences the texture. The (200) α plane for iron was observed for iron rich Fe_3Zn_{13} and Fe_4Zn_6 alloys. The prismatic plane 112, also observed, which can enhance the corrosion resistance. The bcc planes 200 and 110 can improve the hardness and make the alloy electrochemically more noble. The 002 and 102 planes shifted to higher 2θ but 100 plane shifted to lower 2θ, for iron rich deposits. The c/a values with reference to current density was calculated and given in Fig. 3 and it decreases for iron rich deposits. In this the 'c' axis was reduced relatively when compared to 'a' axis and lead to distortion in geometry of the lattice. This shows shrinkage of c–axis is more than a–axis.

3.3 Textural analysis of $Fe_xZn_{(1-x)}$ from sol–gel techniques

Fig. 5. shows some of the X–ray diffraction patterns of the alloy formed under sol–gel method. The alloy obtained under sol–gel method has dominant 002 basal plane for all specimen with a 2θ of 36.496 and d-spacing 2.46 A^o. But 101 pyramidal plane is relatively less intense than that of electrodeposits. This shows the microhardness is relatively lower. Shift over in 2θ values with empirical compositional change was not observed in the sol–gel method and this shows the axial ratio reduction is not significant and distortion of hcp lattice by axial substitution of Fe is lowered. The intensity of planes are relatively higher for zinc rich Fe_2Zn_{15} alloy and both 100, 110 planes for iron is noted for the all samples. The fine structured patterns indicate that the crystallite size is reduced significantly, without internal strain.

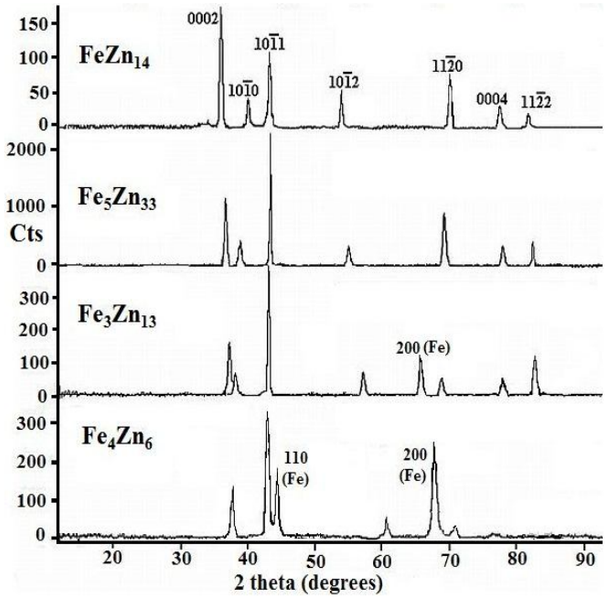

Fig.2 XRD Patterns for $Fe_xZn_{(1-x)}$ Electrodeposits

Shifting over in 2θ values with respect to empirical compositional change was not observed in the sol–gel method and this shows the axial ratio reduction is not significant and distortion of hcp lattice by axial substitution of Fe is lowered. The intensity of planes are relatively higher for zinc rich Fe2Zn15 alloy and both 100, 110 bcc planes is noted for all the samples. The fine structured patterns indicate that the crystallite size is significantly reduced, without internal strain. For zinc rich phases, 110 and 112 prismatic planes are present, with relatively lower intensity, but 004 plane is not observed for these samples.

Approximate crystallite size (in Ao), was calculated by Scherer formula:

$Lhkl = (K \lambda) / (\beta \cos \theta)$

Where, K = Scherrer constant, arbitrary value is about 0.97; β = Full width at half maxima (in radians 2θ);

θ = Diffraction angle for the given hkl plane; λ = Wavelength of X–ray in angstroms.

Similarly average internal strain (ε), can be estimated by Stokes and Wilson formula:

$\varepsilon = \beta / [4 \tan \theta]$.

For Fe6Zn9 for the 002 peak, the estimated Lhkl is about 10.71 Ao with an internal strain co–efficient 0.1175.

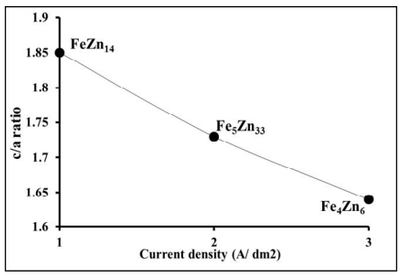

Fig. 3 c/a Data of $Fe_xZn_{(1–x)}$ Electrodeposits

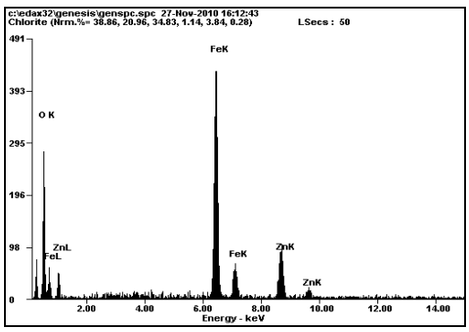

Fig. 4 EDAX for $Fe_xZn_{(1–x)}$ from sol–gel Technique

Table 1. shows the observed lattice parameters c and a of $Fe_xZn_{(1–x)}$ formed under sol–gel method. It must be emphasized that the axial ratio is not declined significantly and this shows the lattice distortion and strain is minimum and this can be elucidated from the SEM images. This shows the either the precipitation of 'η' phase or epitaxial nucleation was not occurred during the alloy formation. Various phases and space groups from the observed empirical composition is given in Table 2. Zinc rich alloys are prevailing with 'η' phase whereas iron rich alloys are mainly forming 'Γ' phase structure. EDAX atomic compositional analysis for the alloy is given in Fig. 4. Based on the empirical composition the phase structure and space group can be correlated.

Table 1: 'c' & 'a' of $Fe_xZn_{(1–x)}$ by sol–gel Method

d–spacing (A^o)	2 θ	hkl	c (A^o)	a (A^o)
2.46	36.4	002	4.92	
2.30	39.1	100		2.65
1.33	70.8	110		2.66
2.08	43.5	101	2.08	2.40
1.43	65.0	200 Fe		3.30
2.03	44.7	110 Fe		4.06

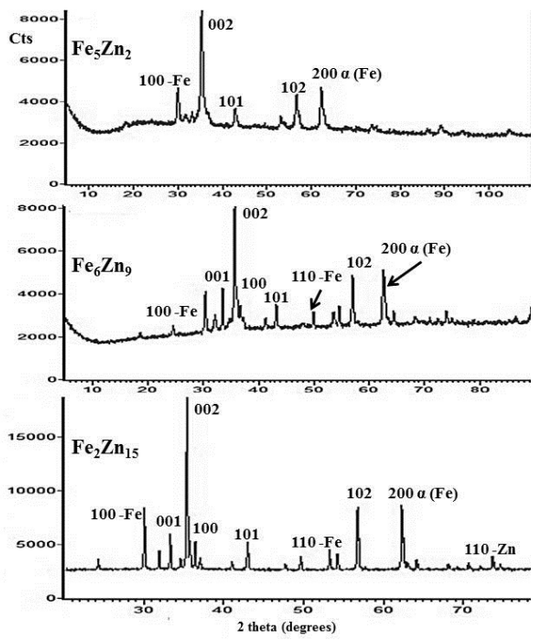

Fig. 5 XRD for $Fe_xZn_{(1–x)}$ from sol–gel Technique

Table 2: Phase Structures of the $Fe_xZn_{(1–x)}$ Alloy

No.	Empirical composition	Phase structure	Space group
1.	$FeZn_{13}$	ζ	C 2/m monoclinic
2.	$FeZn_7$	δ	P63mc hexagonal
3.	Fe_5Zn_{21}	Γ	F43m (I43m) cubic
4.	Fe_2Zn_{37} – $FeZn_{19}$	η	Monoclinic

3.4 Morphological studies

Fig. 6. shows some morphological images of $Fe_xZn_{(1–x)}$ electrodeposits.

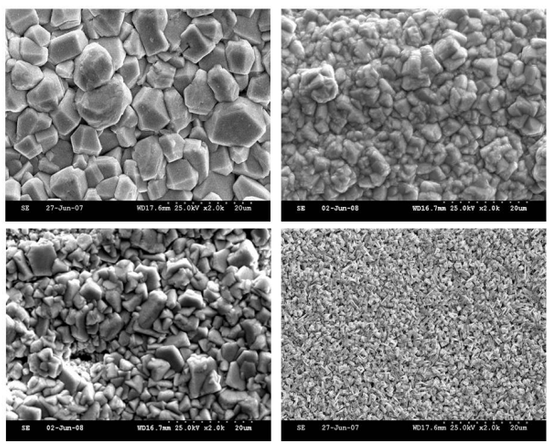

Fig. 6 SEM Images of $Fe_xZn_{(1–x)}$ Electrodeposits

The morphology is entirely depends on the current density as well as empirical composition for electrodeposits. If current density is increased then due to the increase in the nucleation rate than growth rate, fine needle structures were formed. This is because the ad–atoms formed rapidly, which are not undergoing further growth due to the faster deposition kinetics. But at lower current density, nucleation rate is retarded and hence well-defined distorted hcp crystallites are formed. Zinc rich 'η' phase solid solution is forming with hcp morphology, due to the lower axial strain by the partial exclusion of bcc lattice. At moderate current density 'Γ' phase became significant and the deposition rate of zinc is very fast initially and this leads to deplete the Zn^{2+} concentration at the electrode interface, due to the mass-transfer limitations. Therefore, the adsorption of ad–atoms followed by the precipitation of 'δ' phase and iron ad-atoms over previously formed 'η' phase takes place. This leads to the formation of 'Γ' particles and this 'Γ' phase is distinctly noted.

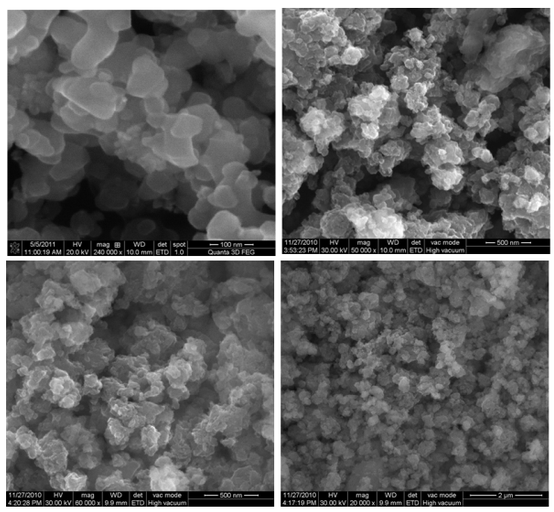

Fig. 7 SEM Images of $Fe_xZn_{(1–x)}$ Alloys from sol–gel Method

Fig. 7 represents some of the morphological characteristics of $Fe_xZn_{(1–x)}$. It can be elucidated that, crystallite size is relatively finer than electrodeposits. The lattice packing is non–coherent with more uniform hexagonal patterns for zinc rich phase. The crystallite size is declined for the $Fe_xZn_{(1–x)}$ with either the increase in temperature or iron content . The relative size varies from 1 nm to 90 nm. For iron rich phases the morphology changes from regular hexagonal to distorted hexagonal.

4. Conclusion

Crystallographic analysis with reference to empirical composition of the $Fe_xZn_{(1–x)}$ alloys formed by both electrodeposition and sol–gel method was investigated. With the increase in current density, iron rich phase was dominant and 101 pyramidal plane with 'δ' (α –Fe) phase structure was obtained. But 002 basal plane was significant with 'Γ' phase structure, for the alloys from sol–gel method. Hexagonal lattice distortion with the reduction in c/a ratio was observed for electrodeposits by the inclusion of bcc lattice. Crystallite size reduction with lower internal lattice strain was noted for alloys from sol–gel technique. For zinc rich phases, 110 and 112 prismatic planes are present, in both types of alloys, but 004 plane is not observed for the alloys from sol–gel method. From

morphological analysis, it can be emphasized that lattice orientation is more uniform with dense packing, for the alloys from electrodeposition technique due to the epitaxial nucleation.

References

1. *Takuya Fujieda, Sachio Takahashi and Shunichi Higuchi, (1992), "Cycling Behaviour of Electrodeposited Zinc Alloy Electrode for Secondary Lithium Batteries", Journal of Power Sources, Vol. 40, 283 - 289.*

2. *Panagopoulos C N, Agathocleous P E, Papachristos V D and Michaelides A (2000), "Sliding Wear Behaviour of Zinc–Iron Alloy Electrodeposits", Surface and Coatings Technology, Vol. 123, 62 - 71.*

3. *Conde A, De Damborenea J, Durán A and Menning M (2006), "Protective Properties of a Sol-Gel Coating on Zinc Coated Steel", Jnl. of Sol-Gel Science and Technology, Vol. 37, 79 - 85.*

4. *Kanagasabapathy M and Sobha Jayakrishnan (2011), Phase Structure and Morphology of Zinc–Iron Alloy Electrodeposits, Journal of Electrochemistry, Vol. 47, 26-33.*

5. *Gomez E, Pelaez E and Valles E (1999), "Electrodeposition of Zinc+Iron Alloys: Analysis of the Initial Stages of the Anomalous Codeposition", Journal of Electroanalytical Chemistry, Vol. 469, 139-149.*

6. *Kanagasabapathy M and Sobha Jayakrishnan, (2011), "Textural and Morphological Studies on Zinc-Iron Alloy Electrodeposits", Journal of Chemical Sciences, Vol. 123, 357 - 364.*

7. *Kanagesan S, Jesurani S, Velmurugan R and Kumar C (2010), "Synthesis of Barium Hexaferrite (BaFe12O19) using D-Fructose as a Fuel", Journal of Manufacturing Engineering, Vol. 5, 133-136.*

8. *International Centre for Diffraction Data (2000), (JCPDS), Database 1- 49, Pennsylvania.*

9. *Kanagasabapathy M and Ramesh Bapu G N K, "FARADAY – Computations" ESTIR– Centre for Electrochemical Sciences, Department of Chemical Engineering, Case Western Reserve University and University of North Carolina, USA.*

